Received: 11 December 2020 | Revised: 5 October 2021 | Accepted: 8 February 2021

DOI: 10.1111/1477-8947.12263

ORIGINAL ARTICLE

NRF NATURAL RESOURCES FORUM WILEY

Responses of sustainable development indicators to human activities and climate change in ecologically fragile areas of impoverished counties in China

Case study of the Zijin Mountain area of Linxian: A national-level poor county

Shanshan Huang[1] | **Chao Ma**[2] | **Pei Liu**[3,4]

[1]School of Surveying and Mapping Land Information Engineering, Henan Polytechnic University, Jiaozuo, China

[2]Key Laboratory of Spatio-Temporal Information and Ecological Restoration of Mines (Ministry of Natural Resources, MNR), Henan Polytechnic University, Jiaozuo, China

[3]Yazhou Bay Innovation Institute, Hainan Tropical Ocean University, Sanya, China

[4]Hainan Academy of Ocean and Fisheries Sciences, Haikou, China

Correspondence
Chao Ma, Key Laboratory of Spatio-Temporal Information and Ecological Restoration of Mines (Ministry of Natural Resources, MNR), Henan Polytechnic University, Jiaozuo 454000, China.
Email: mac@hpu.edu.cn

Pei Liu, Yazhou Bay Innovation Institute, Hainan Tropical Ocean University, Sanya 572000, China; and Hainan Academy of Ocean and Fisheries Sciences, Haikou 570100, China.
Email: cumtlp@gmail.com

Funding information
National Natural Science Foundation of China, Grant/Award Number: U21A20108; Scientific and Technological Innovation Team of Universities in Henan Province, Grant/Award Number: 22IRTSTHN008; Cooperative Exchange Program between the National Natural Science Foundation of China and the

Abstract

Based on Landsat MSS/TM/OLI (1975–2018), MODIS NDVI (2000–2015), and DMSP/OLS (1992–2013) multitemporal remote sensing data, as well as annual average precipitation and temperature data from meteorological stations (1980–2018) and SRTM DEM data, this study extracted information on climate change, human activity, and eco-environmental factors in the Zijin Mountain (ZJM) area of Shanxi Province, and then analyzed the spatiotemporal changes in ecological structure, landscape structure, and climate response. The results revealed that in the ZJM area some sustainable development indicators associated with human activity, ecology, climate, and landscape geography have changed. Specifically, over the 44-year period from 1975 to 2018, the urban and rural construction land area increased by 4.29 times; in the 22-year period from 1992 to 2013, the regional light index has increased by 26.9 times; in the past 32 years, that is, from 1987 to 2018, the average vegetation index of the entire basin increased by about 54.7%, the vegetation cover exhibited a gradual positive trend, and the land use types in the ZJM area were mainly converted from bare land to grassland or forest. Compared with 1987, the area of bare land decreased 32.5% by 2018, whereas the forest and grassland areas increased by 85.7% and 40.7%, respectively. In addition,

Royal Society of UK, Grant/Award Number: 42011530174

over the 44-year period from 1975 to 2018, the road density increased by 8.57 times. The area affected by human activities, comprised roads, urban and rural construction land, and their buffer areas, accounted for 64.87% of the total study area. As a result, the fragmentation index of landscape patches has increased by 6.81 times since 1987. We conclude that in the ZJM area, the ecosystem type has transformed from an indigenous mountainous grassland to mountainous arid agriculture, and from an isolated habitat to a fragmented habitat.

KEYWORDS
climate change, deep poverty mountain area, human-land relationship, landscape fragmentation, Lvliang Mountains, sustainable development goals

1 | INTRODUCTION

The United Nations 2030 Agenda for Sustainable Development (hereafter referred to as the "2030 Agenda") put ending poverty (sustainable development goal [SDG-1]); protecting and restoring water-related ecosystems, including mountains, forests, wetlands, rivers, aquifers, and lakes (SDG-6); making cities and human settlements sustainable (SDG-11); combating climate change and its impacts (SDG-13); and protecting terrestrial ecosystems (SDG-15) into 17 SDGs (United Nations, 2015). Economic poverty and ecological vulnerability are twins (Dong et al., 2003). Due to the economic pressure associated with the elimination of poverty, people tend to rely more on natural resources. Therefore, changes in the human-land relationship are in the same vein as global and regional environmental changes and economic sustainability (Lambin et al., 1999; Turner et al., 1993).

In the scientific community serving the 2030 Agenda, the Group on Earth Observations (GEO), composed of 104 countries and 106 organizations, provides timely, high-quality, long-term, and global information for the monitoring, measurement, and progress assessment of important targets and indicators that are intrinsically linked to sustainable development (Anderson et al., 2017). The preliminary research results of the GEO and the Committee on Earth Observation Satellites have demonstrated that the 40 specific targets and 30 indicators of the 2030 Agenda can be supported by satellite observation technology (Ehrensperger et al., 2019; Q. Zhou et al., 2018). This research involved SDG-2: end hunger, achieve food security, and promote sustainable agriculture (Qi et al., 2018; Qi & Dang, 2018; X. B. Xu et al., 2019); SDG-6: sustainable management of water and sanitation (Madadi et al., 2017; Schmeller et al., 2018; Vörösmarty et al., 2018); SDG-11: sustainable cities and human settlements (Fernandes et al., 2019; Parsa et al., 2019; X. Xu et al., 2018; Zhao et al., 2019); SDG-13: combat climate change and its impacts (Campbell et al., 2018); SDG-14: conserve and sustainably use the oceans, seas, and marine resources (Lu et al., 2018; Mallick & Chakraborty, 2018; Virto, 2018; Visbeck et al., 2014); and SDG-15: protect, restore, and promote the sustainable use of terrestrial ecosystems, sustainably manage forests, combat desertification, halt and reverse land degradation, and halt biodiversity loss (L. B. Liu et al., 2019; Muradyan et al., 2019; Schirpke et al., 2017; Y. Zhou, Huang, et al., 2017; X. Y. Zhou, Lei, & Meng, 2017). It can be seen from this research that the monitoring and evaluation of long-term changes in the regional processes, patterns, and driving forces based on 3S technology has become an effective method for revealing the temporal and spatial changes in land use/cover at the global and regional scales (Acheampong et al., 2018; Holloway & Mengersen, 2018; Kussul et al., 2020).

The hilly and gully region of the Loess Plateau is the area with the most serious soil and water loss in China, and even the world, and its rural residents live in poverty (Dong et al., 2003). Among them, the Lvliang Mountains is one of 14 units of concentrated destitute areas in China (H. Wang et al., 2018). Linxian lies far inland in the Lvliang Mountains and is one of the 585 national-level poor counties in China, and most of its villages are extremely poor. Ecological fragility, a lack of resources and human activities, and natural closure are common characteristics of concentrated destitute areas (H. Wang et al., 2018). The Zijin Mountain (ZJM) area to the northwest of Linxian is an independent geographical unit, surrounded by the Yellow River–Qiushui River–Lvliang Mountains and thus forming an inland island-type closed habitat, which is a natural laboratory and microcosm for studying the global change and ecological evolution of closed inland habitats. The study used 44 years (1975–2018) of remote sensing data and 36 years (1980–2015) of meteorological data and, through a series of preprocessing, obtained information on residential construction land and transportation infrastructure construction land in the region, as well as the time series of the normalized difference vegetation index (NDVI) and normalized difference building index (NDBI). By establishing a sustainable development research framework and comprehensive evaluation index system for fragile ecological environments based on the 2030 Agenda, analyses of the spatiotemporal changes of residential construction land, transportation infrastructure construction land, forest land, NDVI and NDBI in the study area, climate change in the area, and the correlation between the climate–land use–ecological index were made, to obtain objective indicators that can reflect the SDGs of the 2030 Agenda, and to supply scientific references for ecological environment changes and sustainable development in inland poverty-stricken areas, as well as provide suggestions for the revitalization of poor villages.

2 | INDEX SYSTEM

In accordance with the general principles of the United Nations 2030 Agenda, the United Nations Statistics Division has prepared a global indicator framework of various SDGs and targets in the "2030 Agenda for Sustainable Development" (A/RES/71/313&E/CN.3/2018/2&E/CN.3/2019/2). Combining this framework and the characteristics of this study, the following sustainable development research framework (Figure 1) and the multi-factor comprehensive evaluation index system for poverty-stricken mountain resources and environments (Table 1) were designed.

The multi-factor comprehensive evaluation index system was based on the global indicator framework (*) of the 2030 Agenda for Sustainable Development. This study developed a three-level evaluation index system of "target-

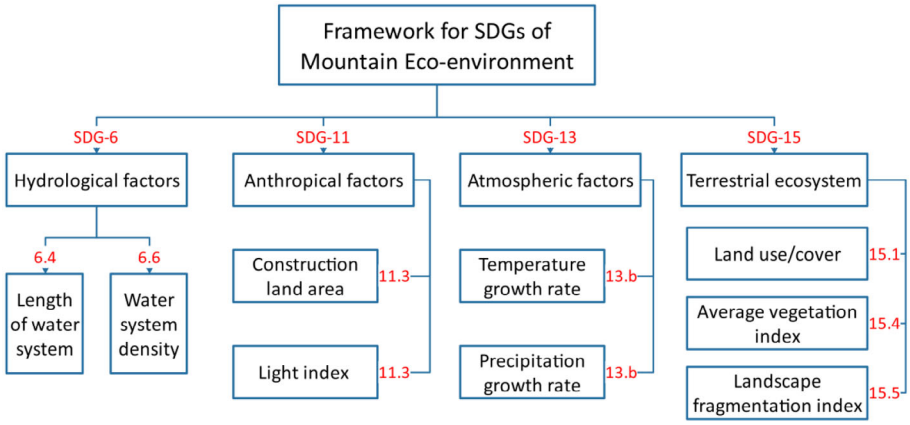

FIGURE 1 Research framework for the sustainable development of mountain resources and environments. SDGs, sustainable development goals

TABLE 1 Dynamic evaluation index system of resources and environments in poor mountainous areas

Goals	Targets (from the 2030 Agenda)	Indicators and interpretation	References
SDG-6 Water and sanitation	6.4 Total length of the water system in the study area (km)	6.4.1 Measures the overall situation of the surface water system in the region.	Juwana et al. (2016)
	6.6 Density of the water system per unit area (km/km^2)	6.6.1 Measures the distribution of surface water systems in the region.	
SDG-11 Cities and human settlements	11.3 22a Light index growth multiple	11.3.1 Measures the degree of regional urbanization.	X. M. Li and Zhou (2018)
	11.3 44a Residential construction land growth multiple	11.3.2 Measures the characteristics of human activities in the region.	X. Y. Zhou, Lei, and Meng (2017); Y. Zhou, Huang, et al. (2017)
SDG-13 Climate change	13.b 36a Temperature growth rate (°C/10a)	13.b.1 Measures the degree of regional temperature changes.	Yin and Sun (2018)
	13.b 36a Precipitation growth rate (mm/10a)	13.b.2 Measures the extent of regional precipitation changes.	
SDG-15 Terrestrial ecosystems, forests, and desertification	15.1 32a Percent reduction in area occupied by bare land (%)	15.1.1 Measures the greening of bare land in a region.	Sun et al. (2019)
	15.1 32a Percent increase in the area of arid grassland (%)	15.1.2 Measures the progress of regional dry grassland management.	
	15.2 32a Percent increase in forest area (%)	15.2.1 Measures progress in regional sustainable forest management.	
SDG-15 Biodiversity	15.4 32a Average vegetation index increase (%)	15.4.1 Measures regional biodiversity coverage.	W. Q. Zhang et al. (2019)
	15.5 32a Mountain ecosystem landscape fragmentation growth multiple	15.5.1 Measures the pressure of regional road development on the ecological environment.	Fang and Wang (2015)

Note: (*) UNECE: Joint UNECE/Eurostat/OECD Working Group on Statistics for Sustainable Development. Available online: https://www.unece.org/stats/groups/wgssd.tor.html (accessed on September 19, 2019).
Abbreviation: SDG, sustainable development goal.

specific target–index." The formulation of the "indicator" evaluation standard, referring to the latest research results in China and abroad, set a five-level evaluation standard of "extremely low, low, moderate, high, extremely high."

3 | MATERIALS AND METHODS

3.1 | Study area

ZJM is located in the northern part of Linxian County, Lvliang City, Shanxi Province, with geographic coordinates of 37°38′–38°22′ N and 110°30′–110°10′ E. The study area is 81.5 km long from north to south, 47.5 km wide from east to west, and covers an area of 2431 km^2.

The study area experiences a continental climate, with an average annual temperature of 8–9°C and average annual rainfall of 300–600 mm. The frost-free period is 150–180 days. It is surrounded by the Yellow River–Qiushui River–Lvliang Mountains and comprises a generally isolated and domed uplift. The main peak of ZJM is 1823 m above sea level. The lowest point is the bed of the Yellow River in the southwest corner (Qikou Town), with an elevation of 700 m. Thus, the difference is as much as 1100 m. The landform type belongs to the typical hilly and gully area of the Loess Plateau, mainly composed of loess-yuan, loess-liang, and loess-mao, and the terrain is broken. Due to long-term carving by running water, the gully is distributed radially around ZJM, and soil and water loss is serious (Figure 2).

The soil in the study area is mainly Quaternary loess, and the soil types are brown earth, cinnamon soil, loessial soil, chestnut soil, and meadow soil (Hao, 2011). The study area is composed of forest, shrubland, arid grassland, sandy land, and bare land, with various types of coverage, which constitute the typical local mountain ecological landscape. The vertical

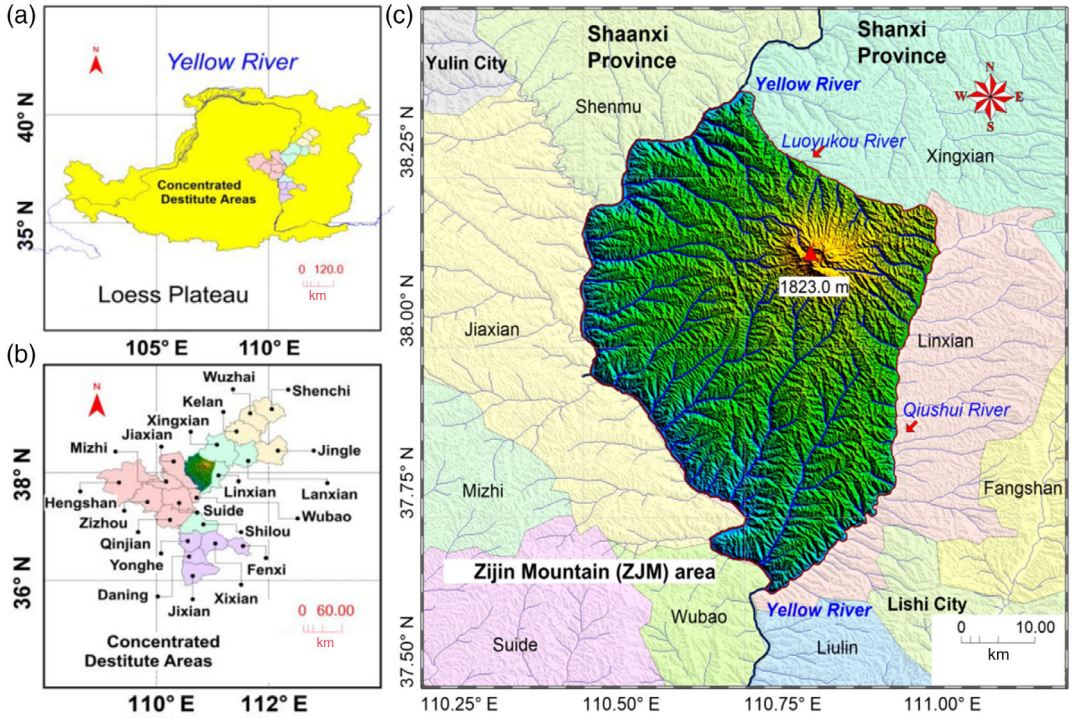

FIGURE 2 Study area and geographic location

zonality distribution of plants according to altitude is pronounced. There are shrubland belts in low-shallow mountains, *Poplar-birch* forest belts and *Larix gmelinii (Rupr.) Kuzen*. forest belts in the middle mountain areas, and *Picea asperata Mast*, *Picea wilsonii Mast*, and *Betula albo-sinensis Burk* in high-altitude distribution areas. The forest is dominated by natural secondary forests of *Larix gmelinii (Rupr.) Kuzen*. and *Pinus tabulaeformis Carrière*. The shrub species mainly include *Lespedeza bicolor Turcz*, *Ostryopsis davidiana Decaisne*, *Spiraea Salicifolia L*., *Hippophae rhamnoides Linn*., and *Rosa xanthina Lindl*., while the herbaceous plants include *Carex tristachya*, *Alkali grass*, and *Artemisia* (Hao, 2011).

3.2 | Research data

The research data included Multispectral Scanner (MSS), Thematic Mapper (TM), and Operational Land Imager (OLI) sensor data consisting of remote sensing images with a resolution of 30–60 m from US Land Resources Satellites (Landsat-2, 5, and 8, hereafter referred to as L2, L5, and L8) from 1975 to 2018 (http://www.usgs.gov); MODIS NDVI data from 2000 to 2018 (https://ladsweb.modaps.eosdis.nasa.gov/search/); and 90-m horizontal resolution Shuttle Radar Topography Mission (SRTM) digital elevation model (DEM) data (SRTM3 DEM, v4.0: http://srtm.csi.cgiar.org/). In addition, there was basic geographic information such as construction land and administrative divisions of 1:250,000 residents in 1999; national meteorological data from the Resource and Environmental Science Data Center of the Chinese Academy of Sciences from 1980 to 2015 (http://www.resdc.cn); and noctilucent data from the Defense Meteorological Satellite Program (DMSP)/Operational Linescan System (OLS) from 1992 to 2013 of the US National Defense Meteorological Satellite Photoelectric Training Program (https://www.ngdc.noaa.gov/eog/dmsp/downloadV4composites.html).

Combined with the cultivation season, plant growth status, climate, and cloud cover, this study selected the remote sensing images from summer and autumn seasons with the best vegetation growth from the available data list, and extracted cultivated land, residential construction land area, NDVI information, and other factors (Table 2).

In the above table, the NDVI was mainly used to analyze the structural changes of surface vegetation cover. The support vector machine (SVM) supervised classification method was primarily utilized for land use/cover change (LUCC) analysis. Among them, the built-up land area in the LUCC included the 4.2 residential land remote sensing interpretation, while the DMSP/OLS data were generally used to examine the development trend of urbanization.

3.3 | Methods and models

By synthesizing the optimized multitemporal data (including remote sensing and terrestrial meteorological data), radiation calibration, atmospheric correction, interpolation and band calculation, multi-temporal vegetation, buildings, lighting, and meteorological information were obtained. As the ecological environment index factors, their time series change characteristics were analyzed. The specific process is illustrated in Figure 3.

The index calculation model involved in Figure 3 is as follows.

1. The NDVI is one of the important parameters reflecting vegetation growth and nutrition information. In remote sensing images, the difference between the reflectivity of the near-infrared band and that of the red band is divided by the sum of the two, that is, the mathematical model of the NDVI is:

$$\mathrm{NDVI} = \frac{\rho_{\mathrm{nir}} - \rho_{\mathrm{red}}}{\rho_{\mathrm{nir}} + \rho_{\mathrm{red}}}. \quad (1)$$

The value range of the NDVI is [−1,1]. Negative values indicate that the ground is covered by clouds, water, snow, and other non-vegetation, which highly reflect visible light; 0 indicates that there is rock or bare soil, and the

TABLE 2 Data sources and uses for the study

Data type	L2 MSS	L2 MSS	L2 MSS	L5 TM	L5 TM	L5 TM	L5 TM	L5 TM	L5 TM	L5 TM	L5 TM	L8 OLI	L8 OLI	L8 OLI	MODIS NDVI[a]	SRTMDEM	DMSP OLS
Acquisition date	1975/08/07	1978/09/23	1981/09/25	1987/08/30	1990/08/22	1993/09/15	1997/08/25	2001/08/20	2004/08/28	2007/09/22	2009/09/27	2013/09/06	2017/08/16	2018/09/04	2000–2018	2000/02/11	1992–2013
Extracted study area	☑	☑	☑	☑	☑	☑	☑	☑	☑	☑	☑	☑	☑	☑	☒	☑	☑
Extracted NDVI	☑	☑	☑	☑	☑	☑	☑	☑	☑	☑	☑	☑	☑	☑	☑	☒	☒
Extracted anthropogenic factors	☑	☑	☑	☑	☑	☑	☑	☑	☑	☑	☑	☑	☑	☑	☒	☒	☑
SVM supervised classification	☒	☒	☒	☑	☑	☑	☑	☑	☑	☑	☑	☑	☑	☑	☒	☒	☒

Abbreviations: DEM, digital elevation model; DMSP, Defense Meteorological Satellite Program; MODIS, Moderate-resolution Imaging Spectroradiometer; MSS, Multispectral Scanner; NDVI, normalized difference vegetation index; OLI, Operational Land Imager; OLS, Operational Linescan System; SRTM, Shuttle Radar Topography Mission; SVM, support vector machine; TM, Thematic Mapper.

[a]MODIS NDVI data were from 2000 to 2018, collected on August 12 or 13.

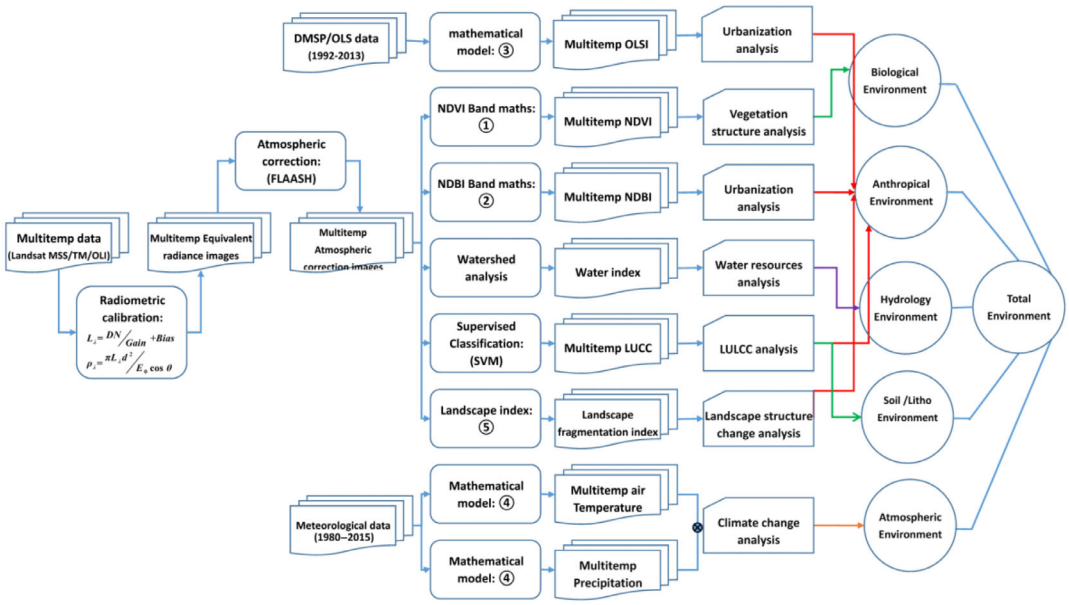

FIGURE 3 Flow chart of extraction and analysis of ecological environment index factors. DMSP, Defense Meteorological Satellite Program; MSS, Multispectral Scanner; NDBI, normalized difference building index; NDVI, normalized difference vegetation index; OLI, Operational Land Imager; OLS, Operational Linescan System; SVM, support vector machine; TM, Thematic Mapper

reflectivity is approximately equal; positive values indicate that there is vegetation cover, and increase with increasing coverage.

2. The NDBI can accurately reflect construction land information. The larger the value, the higher the proportion of residential construction land, and the higher the building density. The mathematical models of the NDBI consist of the following.

For the remote sensing images of the Landsat TM/ETM+ sensors:

$$\mathrm{NDBI} = \frac{\rho_{\mathrm{mir}} - \rho_{\mathrm{nir}}}{\rho_{\mathrm{mir}} + \rho_{\mathrm{nir}}}, \tag{2a}$$

where ρ_{mir} and ρ_{nir} are the spectral reflectance of the fifth and fourth bands of the Landsat TM/ETM, respectively.

For the remote sensing images of the Landsat 8 OLI sensor:

$$\mathrm{NDBI} = \frac{\rho_{\mathrm{swir}} - \rho_{\mathrm{nir}}}{\rho_{\mathrm{swir}} + \rho_{\mathrm{nir}}}. \tag{2b}$$

In this formula, ρ_{nir} and ρ_{swir} are the spectral reflectance of the fifth and sixth bands of the Landsat 8 OLI, respectively.

3. DMSP/OLS nighttime light images are closely related to road traffic, urban and rural residential areas and population centers, social and economic development, and other information. The mathematical model of DMSP/OLS light data extraction after correction is:

$$L_{\text{annual}} = \frac{\sum_{1}^{n} L_{\text{index}} \cdot \text{pixel}}{n}. \quad (3)$$

In this formula, L_{index} is the digital number (DN) value of the light image, and n is the total number of pixels.

4. The spatial interpolation dataset of the annual average temperature and annual precipitation in China since 1980 is based on daily observation data from more than 2400 meteorological stations nationwide, and is generated through collation, calculation, and spatial interpolation processing. The annual average temperature unit is 0.1°C, and the annual precipitation unit is 0.1 mm. The mathematical model for temperature and precipitation extraction is

$$T_{\text{annual}} = \frac{\sum_{1}^{n} T_{\text{pixel}}}{n} \times 0.1;\ P_{\text{annual}} = \frac{\sum_{1}^{n} P_{\text{pixel}}}{n} \times 0.1, \quad (4)$$

where T_{pixel} and P_{pixel} are the temperature and precipitation image DN values, respectively, and n is the total number of pixels.

5. The landscape patch fragmentation index refers to the fragmentation degree of landscape segmentation, reflecting the complexity of landscape spatial structure. As the interference of human factors intensifies, the landscape patch fragmentation index increases, and the increase in the number of landscape patches has a great impact on the landscape patch fragmentation index. The calculation formula is the following:

$$FN_1 = \frac{(N_p - 1)}{N_c} \quad (5)$$

In this formula, FN_1 is the landscape fragmentation index of the entire study area, N_p is the landscape patch index, and N_c is the ratio of the total study area to the smallest patch area; $FN_1 \in [0,1]$, where 0 means that the landscape is not destroyed and 1 means that the landscape is completely destroyed.

4 | RESULTS ANALYSIS

4.1 | Time series NDVI mapping

Affected by the orbital period of the archived data and the amount of cloud, it is difficult to obtain data with the same imaging time (simultaneous phase). In this study, multispectral data with approximately equal time intervals (3–5 years) and the best period of vegetation growth (August–September) were selected. Through multi-spectroscopic image synthesis, radiation calibration, atmospheric correction, and band math (Equation (1)), 14 NDVI images of the region with a time span of 44a (1975–2018) were obtained (Figure 4).

The study area consists of forest, shrubland, arid grassland, sandy land, bare land, and other land cover types, which constitute the typical ecological landscape (Hao, 2011). Based on this, six-level density segmentation was performed on the NDVI results, in which the six levels comprised the extremely high vegetation coverage interval

(0.8, 1.0], the high vegetation coverage interval (0.6, 0.8], the medium vegetation coverage interval (0.4, 0.6], the low NDVI vegetation coverage interval (0.2, 0.4], the very low vegetation coverage interval (0.0, 0.2], and the non-vegetation coverage interval [−1.0, 0.0], to obtain a macro-level understanding of the proportion of each interval (Figure 4).

4.2 | Time series NDBI mapping

This research performed color synthesis, false color synthesis, enhancement, and image fusion on Landsat MSS/TM/OLI multispectral data from 1975 to 2018, obtaining 14 moderate-resolution (30 m and 60 m) images. Under the GIS platform, these images were superimposed with the basin scope, combined with the NDBI calculation results (Equations (2) and (2)), and through research, judgment, and human-computer interactive interpretation, the residential construction land boundaries in proportions that are highly relevant to human activities were extracted (Figure 5).

From this figure, it can be seen that from 1975 to 2004 the number of settlements and the amount of construction land exhibited slow increasing trends, while from 2007 to 2013 these factors displayed rapid increasing trends, and from 2017 to 2018 the growth rate slowed but tended to aggregate. In the southern part of the ZJM area, Linxian on the banks of Qiushui River, Kehu Town on the east bank of the Yellow River, and Qikou Town at the confluence of the Qiushui River and Yellow River each contain large-scale residential areas.

4.3 | Residential area remote sensing interpretation time series mapping

DMSP/OLS images acquire information about the intensity of light at night, and this light intensity is closely related to the development of towns. Nighttime light images can be used as a representation of human activity and have become a good data source for human activity monitoring research (D. R. Li & Li, 2015). With the support of ArcGIS©, the DMSP/OLS remote sensing light data from 1992 to 2013 were radiation corrected and reprojected (WGS 1984 UTM Zone 49 N), and band math was then performed (Equation (3)), thereby obtaining 22 years of nighttime light images with a resolution of 500 m (Figure 6).

The DMPS/OLS nighttime light images took towns as the target areas, which could better reflect the characteristics of human activities, and then expressed the shape and contour information of towns, thus providing accurate, direct, and efficient technical means for town expansion monitoring (D. R. Li & Li, 2015). There was no saturation phenomenon in the entire study area, and this investigation conducted a six-level density division of the brightness of the nighttime light images (Figure 6). In the early nighttime light images, only four town areas were distributed in blocks, namely Linxian, Sanjiao, Qikou, and Kehu. Linxian, Sanjiao, and Qikou then gradually merged into a line, presenting a distribution state of one point (Kehu Town) and one line. After 2009, with the construction of the S50 expressway, Linxian and Kehu were connected by the expressway, and a light belt appeared in the center of the research area. Currently, a residential gathering belt intersected by a vertical line (consisting of Linxian, Sanjiao, and Qikou) and a horizontal (E–W) line (S50) has formed.

4.4 | Time series LUCC mapping

The years 1975, 1978, and 1981, were negatively impacted by data quality, and the resolution was low, making it difficult to distinguish various types of features. Therefore, except for the three phases of the Landsat MSS data, the other original images were preprocessed, and this study utilized the SVM method to supervise classification of the

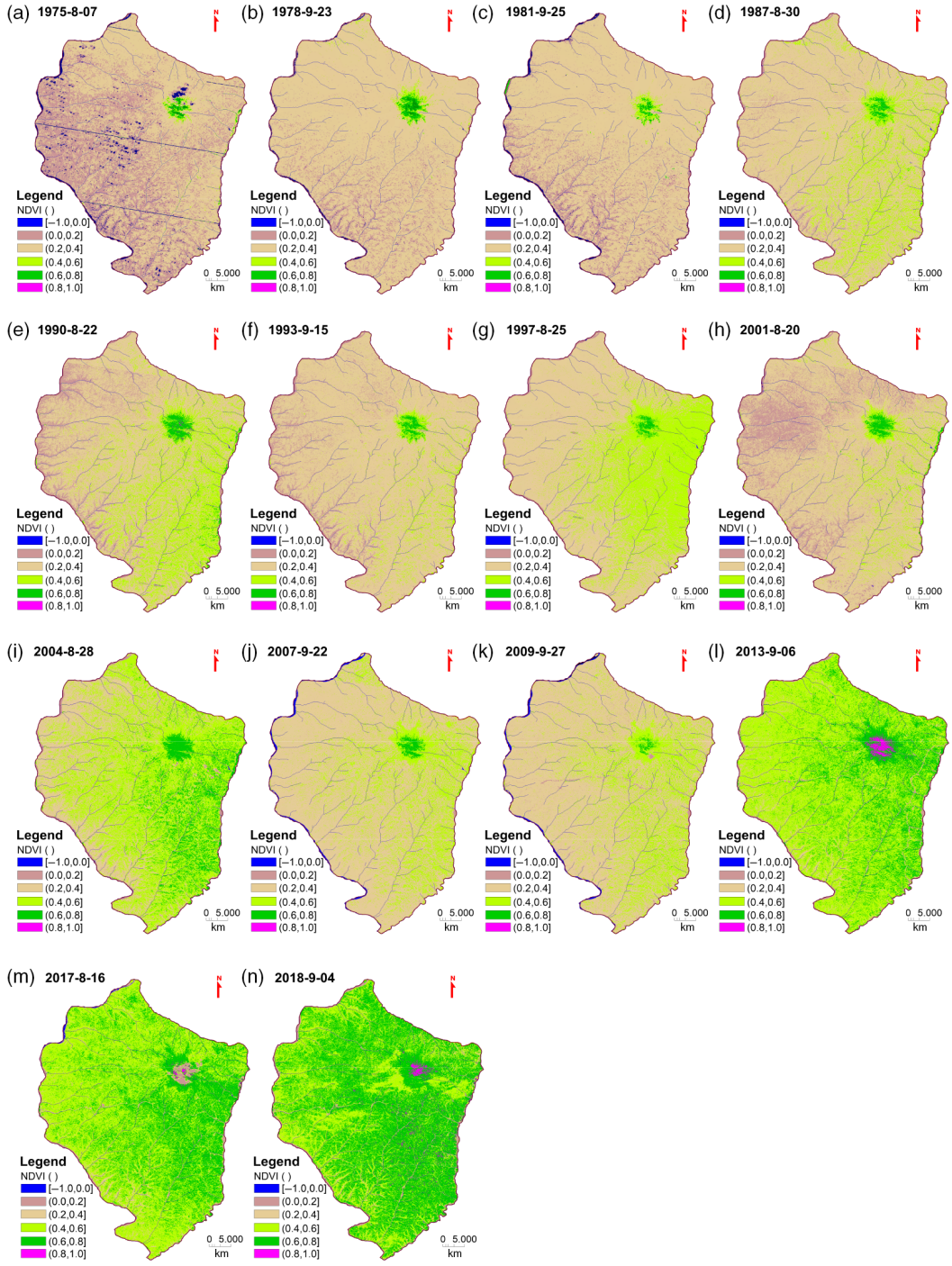

FIGURE 4 Time series normalized difference vegetation index (NDVI) density segmentation mapping

Landsat remote sensing images from 1987 to 2018. After accuracy verification, each land use type was converted into a vector, and 11 phases of LUCC images with a time span of 32a (1987–2018) were obtained for the study area (Figure 7).

This investigation used the IGBP GLCC Version 2.0 global land cover classification system to divide the study area into six land use types: water, grassland, cropland, forest, built-up land, and bare land. It can be seen that the forest in the study area is mainly distributed on top of ZJM. The grassland mainly forms a mosaic spatial pattern with the forest and cropland, and has exhibited an expansion trend. From 1987 to 2009, the built-up land was mainly concentrated along the banks of the Qiushui River and the Yellow River Basin. After 2009, with the development of urbanization, the built-up land was mainly distributed in the southern part of the ZJM area and displayed a tendency to aggregate.

The post-processing utilized principal component analysis and cluster analysis to remove small spots, ultimately obtaining the classification results, and then employed the confusion matrix method to evaluate accuracy. The evaluation results are listed in Table 3.

Table 3 shows that the kappa coefficients of the 11-stage image classification results obtained in this study were all >0.9, and the overall accuracy was also >99%. Therefore, the accuracy of the image classification results meets the requirements.

5 | DISCUSSION

5.1 | Analysis of the change in vegetation cover structure

The remote sensing vegetation index is one of the most important indicators of ecological environment change and is positively correlated with the fraction of photosynthetically active radiation by the vegetation canopy, net primary production, vegetation cover, and other biophysical characteristics of vegetation (Myneni et al., 2001). This study classified and counted the number of pixels in each level of the time series NDVI, and then multiplied the result by the resolution to obtain the areas of the various levels of surface vegetation cover (Table 4).

The percentage of the average NDVI area in the ZJM basin over the 44a study period (1975–2018) revealed that the area with an NDVI value <0.2 gradually decreased and averaged 24.8%; for the NDVI interval (0.2, 0.4], the area increased initially and then decreased and its 44a-average was the highest reaching 40.7%; for the intervals (0.4, 0.6] and (0.6, 0.8], the NDVI areas displayed gradual increasing trends with average values of 25.3% and 9.0%, respectively; while the proportion of average area with an NDVI value >0.8 was extremely low, < 1%.

It should be noted that from 1975 to 1981, due to the influence of data quality, bare land occupied a large area. Therefore, apart from this period of Landsat MSS NDVI data, only vegetation cover changes from 1987 to 2018 were analyzed, and the MODIS NDVI data from 2000 to August 2018 were used for verification (Figure 8).

The classification percentage histogram was used to qualitatively express the macro-ecological structural changes of vegetation in the ZJM basin. The 32a (1987–2018) vegetation NDVI of the ZJM basin gradually changed from low coverage to high coverage. The IBM SPSS© comparison tool was used to analyze the August results of the MODIS NDVI (2001, 2004, 2007, 2009, 2013, 2017, and 2018) in the same year. The SPSS© Pearson correlation coefficient was $r = .9386$ (significance test $p < .001$, sample size $n = 7$), and the change trends of the MODIS NDVI and Landsat NDVI were highly consistent.

5.2 | Analysis of anthropogenic factors

5.2.1 | Urban–rural residential construction land change

The change in the area of residential construction land is an indicator closely related to human activities, and one of the human dimensions that can be expressed through remote sensing images. To collect objective evidence of

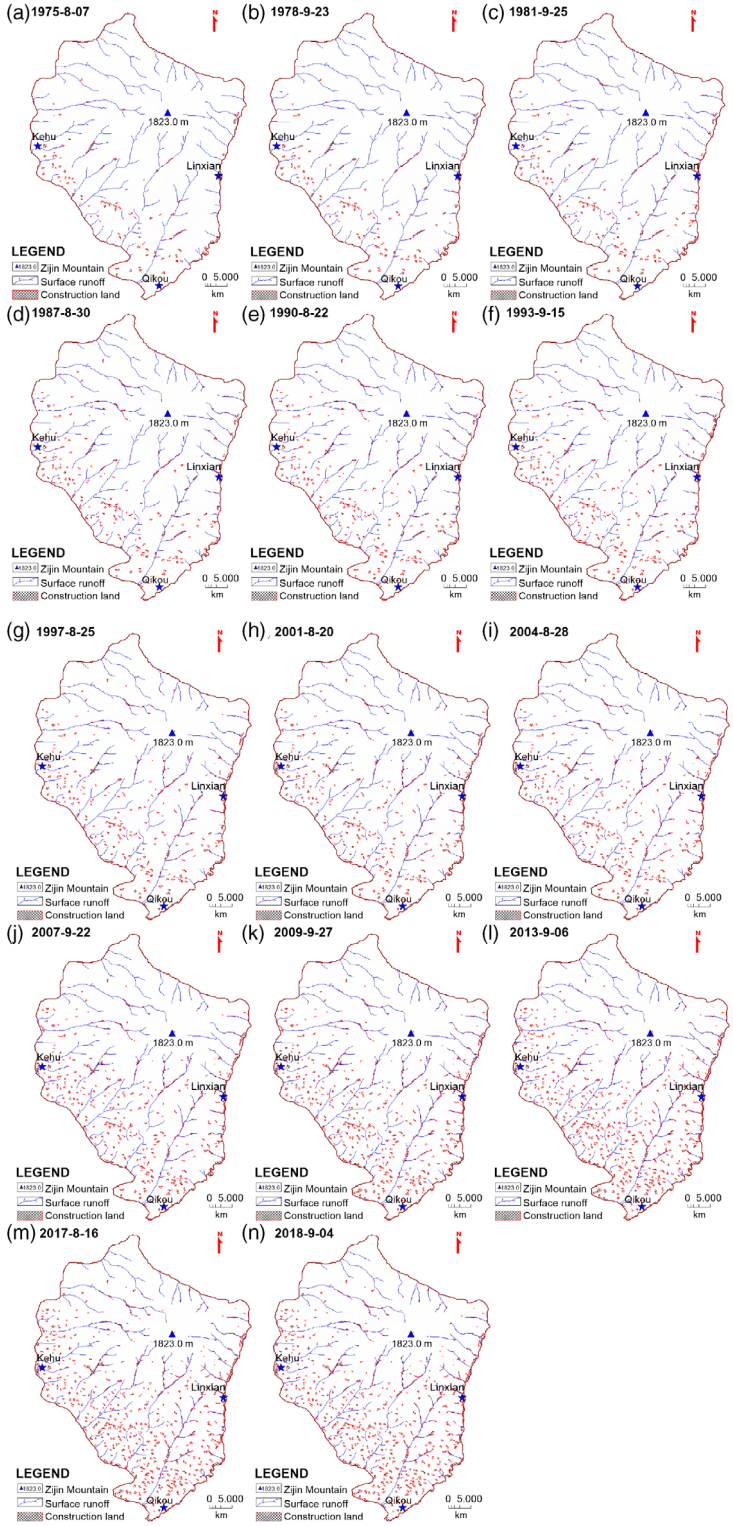

FIGURE 5 Remote sensing interpretation results of residential construction land in the study area

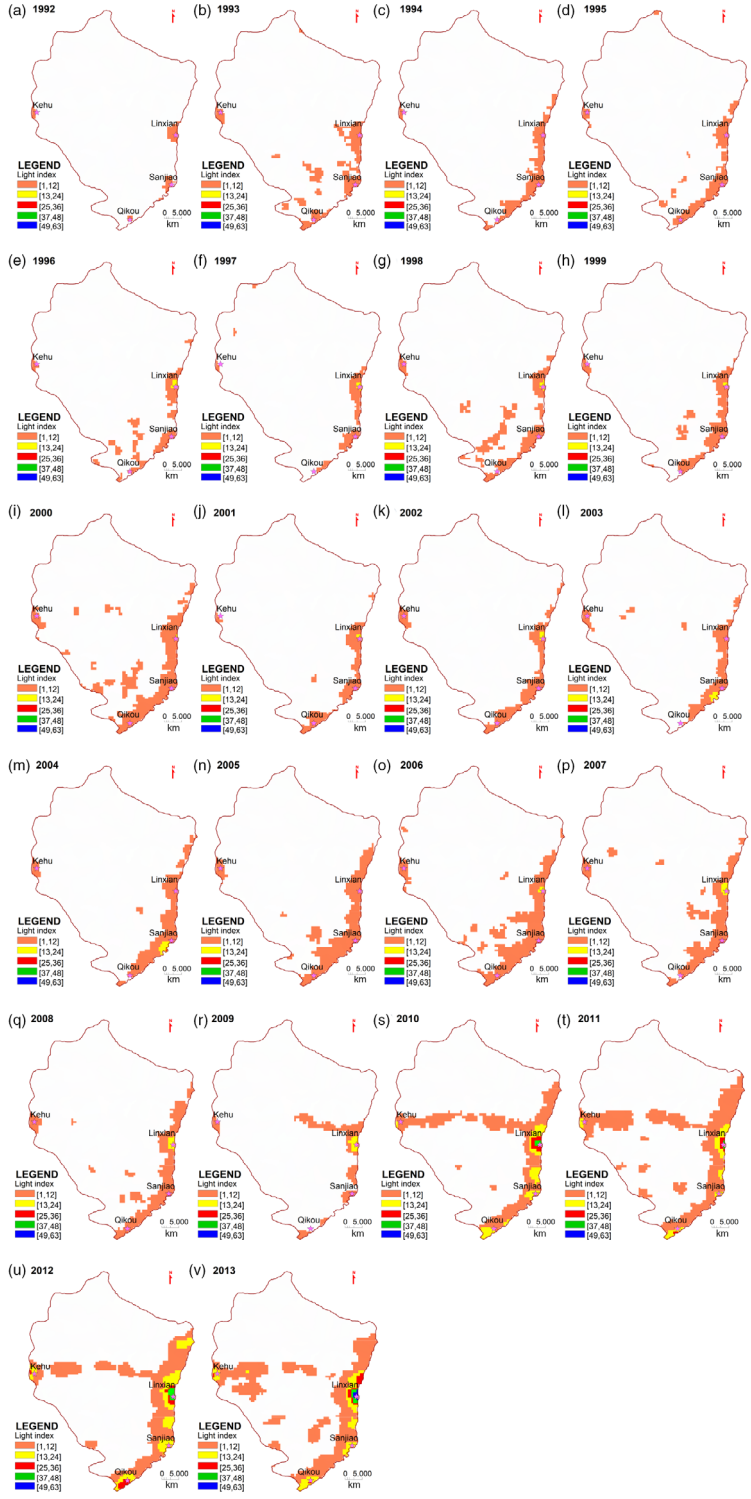

FIGURE 6 Time series of nighttime light images from the Defense Meteorological Satellite Program satellite constellation (1992–2013)

enhanced human activities over the 44a study period, information on the number and area of patches of real-type (in proportion) residential construction land in the ZJM basin from 1975 to 2018 was extracted (Table 5).

The number of building patches and area change line charts express the spatiotemporal changes of human activities. The number of building patches is a direct manifestation of the increase in residential settlements (Figure 9). The area of construction land for actual residents in the ZJM basin increased from 17.88 km^2 in 1975 to 76.67 km^2 in 2018. The number of patches of construction land for residents increased by 6.04 times over the 44a period, and the area of construction land expanded by 4.29 times.

The increase in the number of building patches from the early stage demonstrates that the range of human development of natural resources has expanded. In addition, the increase in the number of patches slowed in the later period while the area continued to increase, indicating that the degree of urbanization had increased. The evaluation results of the development level of new-type urbanization revealed that the spatial distribution of new-type urbanization in different cities in Shanxi Province vary quite a bit, displaying a high level of urbanization in the central region and gradually decreasing in the surrounding areas. The urbanization of Lvliang City is currently at a moderate level (Z. G. Du, 2018).

5.2.2 | Remote sensing light brightness index change

Nighttime light intensity information and changes in light area can be used as indicators of the degree of urbanization and human activities (Q. L. Zhang et al., 2016), thus providing objective evidence for the evolution of urbanization and the footprint of human activities. This study extracted night light index and area information from 1992 to 2013 in the ZJM area (Table 6).

From 1992 to 2014, the sum of the lighting area and light index time series exhibited fluctuations followed by a rising trend (Figure 10). The light brightness area was the smallest in 1992; there were brief decreases in 2001 and 2009; and the overall increase trend of light area was significant from 2010 to 2013. The sums of the lighting area and light index in 2013 were 14.4 times and 26.9 times their respective 1992 values.

The literature shows that in 2000 in Linxian County and other areas northwest of Lvliang, the county urbanization level was at its lowest. In 2010 the urbanization strategy was being vigorously promoted in Shanxi Province, and by 2012, the overall urbanization level had been improved, especially in Lvliang City, with multiple county-level urbanization core areas appearing, although Linxian County was still developing slowly (Yang & Zhao, 2015).

5.3 | LUCC analysis

LUCC is an intuitive manifestation of the joint action of human activities and natural factors. As the core content of the International Geosphere-Biosphere Programme and the International Human Dimension Programme on Global Environmental Change, LUCC is an important driving force behind the study of changes in the global ecological environment (J. Y. Liu et al., 2018). Understanding the characteristics of LUCC to regulate human activities and achieve rational land use is the only way to achieve regional sustainable development. This study performed change detection on the image classification results, obtained the transformation relationships between various land use types, and converted the transformation area between each type into a Sankey diagram (Figure 11).

It can be seen from this figure that the conversion of land types mainly occurred between bare land, grassland, forest, and built-up land. The areas of grassland and forest fluctuated dramatically. These areas reached their peaks in 2018, accounting for 14.45% and 22.78% of the study area, respectively, with the transfer mainly from bare land. From 1987 to 2007, bare land exhibited a slight growth trend, mainly from grassland. From 2009 to 2018, bare land displayed a large decrease in area. During three stages, that is, 2009–2013, 2013–2017, and 2013–2018, 125.77, 141.24, and 142.2 km^2 were converted into grassland, respectively; at the same time, 134.85, 263.43, and

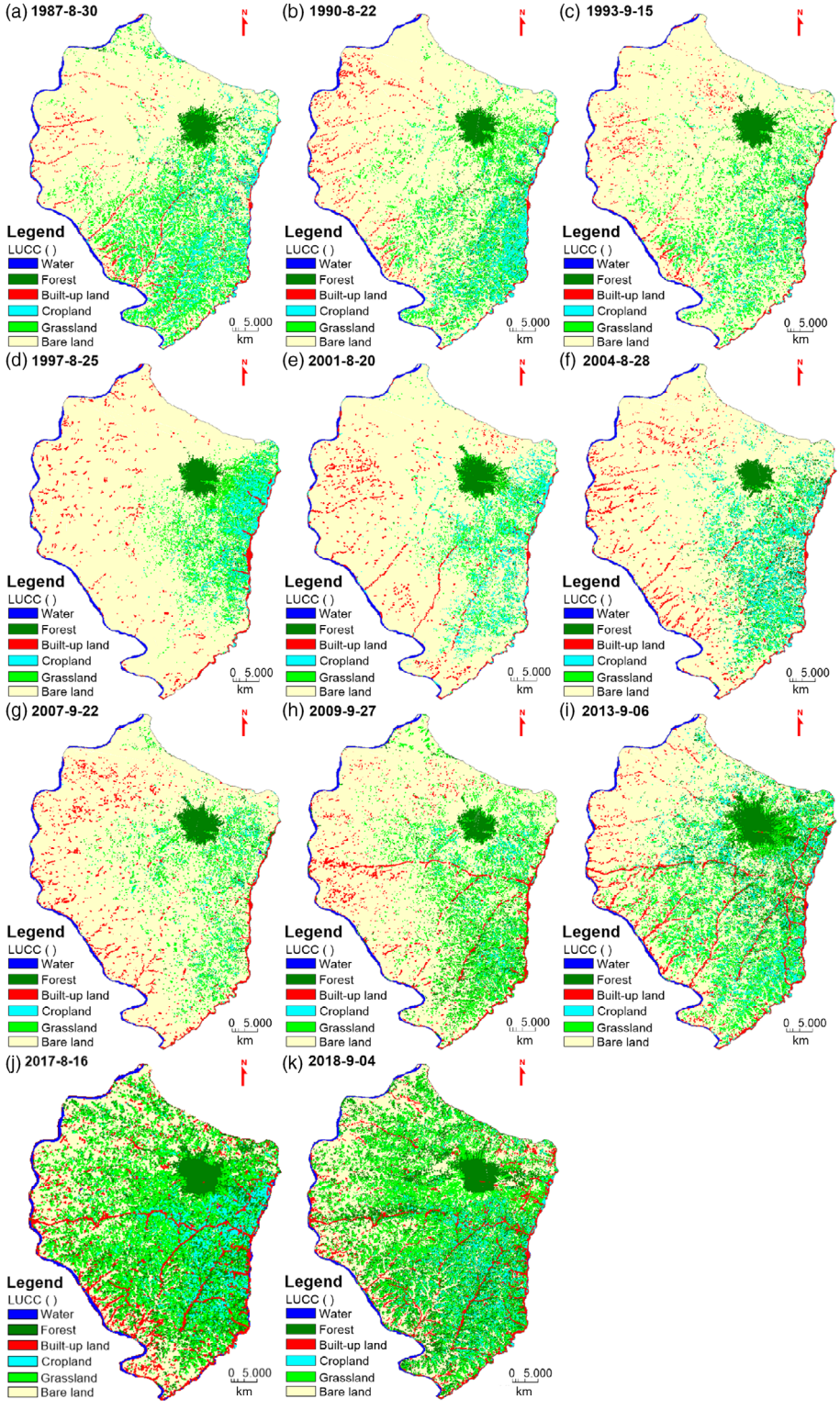

FIGURE 7 Time series land use classification mapping in the study area. LUCC, land use/cover change

TABLE 3 Accuracy evaluation results

Year	1987	1990	1993	1997	2001	2004	2007	2009	2013	2017	2018
Overall accuracy (%)	99.98	99.95	99.98	99.89	99.94	99.97	99.89	99.96	99.78	99.91	99.97
Kappa coefficient	0.9917	0.9883	0.9939	0.9767	0.9875	0.9885	0.9802	0.9855	0.9635	0.9863	0.9887

TABLE 4 Statistics from normalized difference vegetation index density slices (unit: Percent)

Segmentation grade	1975/08/07	1978/09/23	1981/09/25	1987/08/30	1990/08/22	1993/09/15	1997/08/25	2001/08/20	2004/08/28	2007/09/22	2009/09/27	2013/09/06	2017/08/16	2018/09/04	44a average
[0.0, 0.2]	97.5	97.3	98.1	4.5	10.8	8.6	1.9	19.2	2.1	0.6	1.6	1.8	1.7	1.6	24.8
(0.2,0.4]	2.2	2.4	1.8	76.7	62.0	84.1	63.9	71.1	36.8	76.5	74.6	7.9	5.7	3.4	40.7
(0.4,0.6]	0.3	0.3	0.1	18.0	25.3	6.5	33.6	8.5	49.6	22.1	23.3	66.9	59.8	40.3	25.3
(0.6, 0.8]	0.0	0.0	0.0	0.8	1.8	0.8	0.6	1.1	11.6	0.8	0.5	22.5	32.5	53.4	9.0
(0.8, 1.0]	0.0	0.0	0.0	0.0	0.1	0.0	0.0	0.0	0.0	0.0	0.0	0.8	0.2	1.3	0.2

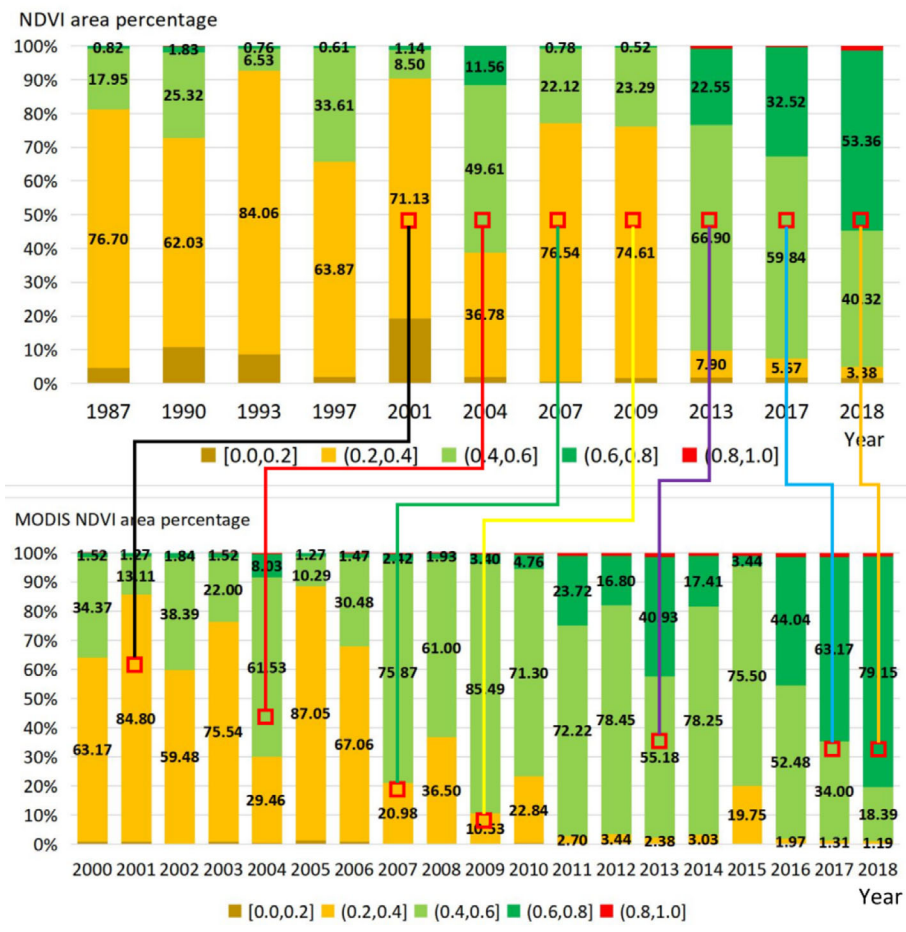

FIGURE 8 Time series of vegetation cover change mapping in the study area. MODIS, Moderate-resolution Imaging Spectroradiometer; NDVI, normalized difference vegetation index

197.66 km^2 were converted into forest, while the bare land area experienced a significant decrease of 33.89% during the three-stage period. The transfer-in rate of built-up land within the 32a period 1987–2018 was greater than the transfer-out rate, with the area increasing from 24.85 km^2 in 1987 to 77.06 km^2 in 2018, representing a net increase of 52.26 km^2 and an annual growth rate of 2.55 km^2/a. The water in the study area was mainly the Yellow River, which exhibited a slight overall downward trend. With the exception of the frost periods in 1993, 2007, and 2009, the cropland area displayed no significant changes during the study period.

5.4 | Climate change analysis

With the support of ArcGIS© software, the spatial interpolation datasets of the national average annual temperature and annual precipitation from 1980 to 2015 were reprojected (WGS 1984 UTM Zone 49 N) and quantitatively calculated (Equation (4)) as the annual average temperature and precipitation in the study area (Figure 12).

The following can be discerned from this figure:

TABLE 5 Change of urban–rural construction land in the Zijin Mountain basin from 1975 to 2018

Acquisition date	1975/08/07	1978/09/23	1981/09/25	1987/08/30	1990/08/22	1993/09/15	1997/08/25	2001/08/20	2004/08/28	2007/09/22	2009/09/27	2013/09/06	2017/08/16	2018/09/04
Area of construction land (km^2)	17.88	20.99	26.03	31.49	35.41	38.45	39.36	43.78	44.79	52.02	61.66	74.79	76.38	76.67
Number of construction land patches	97	123	154	212	249	267	297	320	329	382	449	556	580	586

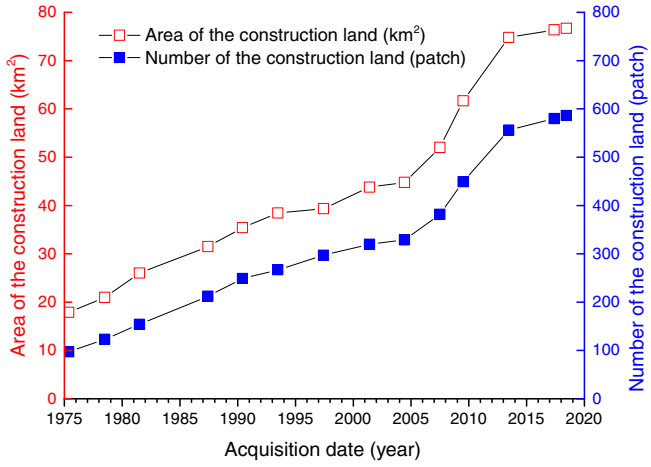

FIGURE 9 Change trend of urban–rural residential construction land

From 1980 to 2015, the average annual temperature in the study area displayed a gradual upward trend, as seen in Figure 12a.

The 36a average temperature was 9.9°C. The phased statistical results revealed that the average of the stages from 1980 to 1989, 1990 to 1999, 2000 to 2009, and 2010 to 2015 were 9.2, 9.9, 10.3, and 10.2°C, respectively, and the temperature increased significantly. It can be seen from the temperature histogram that 1996 was the inflection point of temperature changes. The temperatures in most of the previous 17 years were lower than the average, and the temperatures continued to increase in the 19 years from 1997 to 2015, 15 years of which were above average. The minimum temperature of the 36a period occurred in 1984 (8.4°C). The year 1999 was the warmest during the observation period, with an average annual temperature of 11.1°C. The tendency rate of temperature increase during the 36a period was 0.42°C/10a.

From 1980 to 2015, the annual precipitation in the study area showed a fluctuating upward trend, as seen in Figure 12b.

According to the fluctuating precipitation graph, the amplitude of fluctuations in the early period was small, while the fluctuations in the middle and late periods increased significantly. The annual average precipitation during the 36a period was 461.4 mm. There were 4 years with relatively obvious low values: 1997 (357.1 mm), 1986 (353.0 mm), 2005 (325.2 mm), and 1999 (303.2 mm). Meanwhile, there were 6 years with relatively high values: 2011 (577.2 mm), 2012 (577.9 mm), 1985 (579.9 mm), 1988 (595.1 mm), 2007 (595.2 mm), and 2009 (626.7 mm), and there were more years of continuous flooding and drought. These findings are consistent with previous analysis results (F. Li et al., 2015). Based on the segmented average plot of precipitation, the annual precipitation can be divided into four stages. The phased statistical results revealed that the mean values of the phases from 1980 to 1987, 1988 to 1996, 1997 to 2006, and 2007 to 2015 were 439.6, 480.3, 399.3, and 530.9 mm, respectively, with annual precipitation exhibiting an 8–10-year cycle. The tendency rate of precipitation increase during the 36a period was 18.7 mm/10a.

Climate change is affected by many factors and is not simply a linear change process. The IPCC5 attributed the most important influencing factors of climate change to human activities (Qin et al., 2014). Under the current general trend of global warming, the ZJM area is extremely sensitive to climate change, and its tendency rate of temperature increase is exceeding the rate of temperature rise calculated on a large spatial scale. For example, the global (land and ocean) temperature increase rate was 0.117°C/10a (1951–2012) (IPCC, 2013), the average annual temperature increase rate for China was 0.274°C/10a (1960–2016) (Q. Q. Du et al., 2018), and the average temperature increase trend in Shanxi Province was 0.295°C/10a (1959–2008) (M. B. Wang & Fan, 2009).

TABLE 6 Time series of remote sensing light brightness index change from 2000 to 2013

Acquisition date	1992	1993	1994	1995	1996	1997	1998	1999	2000	2001	2002
Lighting area (km^2)	39.20	173.17	136.04	156.03	134.23	88.01	200.95	164.08	316.48	131.63	158.37
Sum of the light index (number of pixels × brightness)	766	2465	2148	2840	2413	1595	2904	2409	4396	2357	3299
Acquisition date	**2003**	**2004**	**2005**	**2006**	**2007**	**2008**	**2009**	**2010**	**2011**	**2012**	**2013**
Lighting area (km^2)	156.03	204.32	269.23	315.18	245.34	245.08	134.74	417.22	521.32	497.44	565.98
Sum of the light index (number of pixels × brightness)	2945	3764	4147	6179	5351	5208	4525	15,664	14,650	20,553	20,596

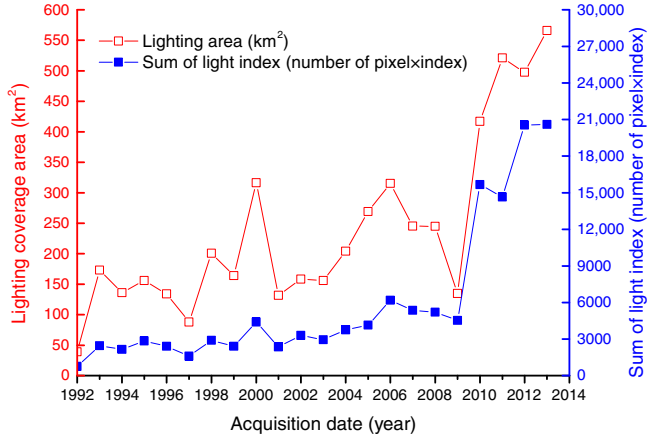

FIGURE 10 Trend of the remote sensing light index change

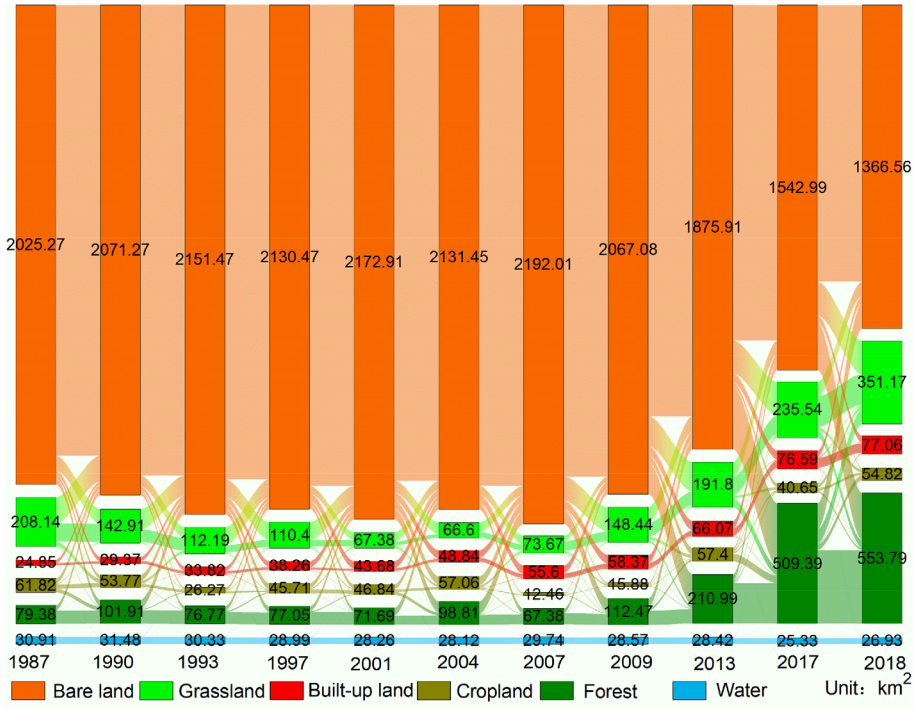

FIGURE 11 Time series of land use/cover change analysis in the study area

5.5 | Analysis of landscape fragmentation caused by roads

Landscape fragmentation is one of the main reasons for the decline of biodiversity and is mainly manifested as affecting the genetic exchange between populations or communities, changing the geographical environment required for species survival, reducing the living space required by species, and altering the structure of the ecosystem (Hu et al., 2005; Van der Ree et al., 2011). Fragmentation is a typical landscape feature of the Loess Plateau (Z. G. Li et al., 2005). The ZJM area not only is a ravine that has been carved by natural forces but has also been

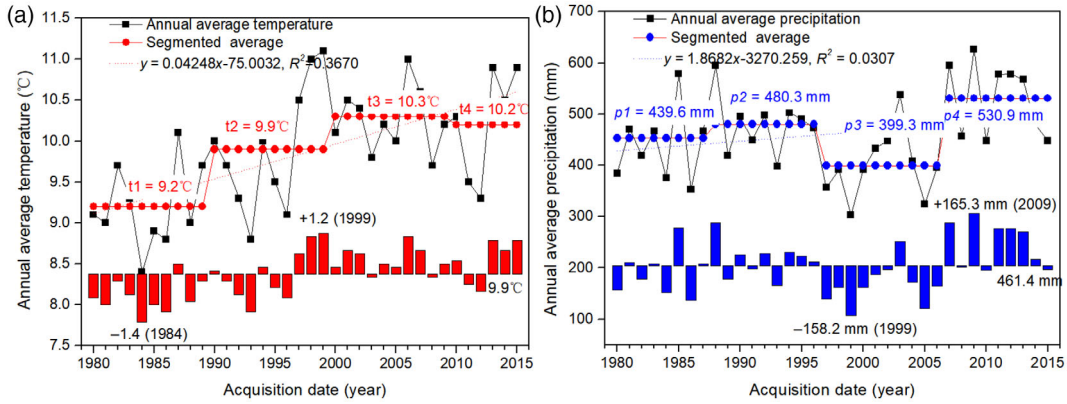

FIGURE 12 Trends of temperature and precipitation in the Zijin Mountain area from 1980 to 2015

fragmented by roads. According to the interpretation of 2018 remote sensing images, the roads in the ZJM area mainly consist of expressways, trunk highways, railways, county roads, and township roads, as seen in Figure 13a. In 1975, the total road length was 156.2 km, and the road density was 0.07 km/km^2; by 2018, the total road length was 1470.5 km, and the road density reached 0.60 km/km^2. Thus, during this 44a period road density increased by 8.57 times.

The direct effects of roads on the landscape are as follows: the number of patches increases and their area decreases, their shapes tend to be irregular, the area of inland habitat shrinks, the corridor is cut off, and the patches are isolated from each other. In addition, the impact of roads on the landscape is much greater than the roads themselves. With reference to the sensitivity ranges of wild animals and plants to different roads in road ecology, this study used 1.5-km extrapolations of railways and expressways in the ZJM area as their biological impact zones (M. Y. Li et al., 2012; S. Li et al., 2018), and analogously used 1.5-km extrapolations of trunk highways (Benítez-López et al., 2010), 0.5-km extrapolations of county roads and residents outside (Boarman & Sazaki, 2006), and 0.25-km extrapolations of rural roads as their biological impact zones (Feng et al., 2019). The different road impact zones were then combined to form a human activity impact area. The roads sliced up the landscape matrix. The total buffer area was 1243 km^2, accounting for 51.13% of the total study area, with landscape occupying more than half of this area, as seen in Figure 13b. Under the effect of the settlement buffer area, as seen in Figure 13c, the landscape matrix was perforated. The road buffers were further superimposed and merged into a human activity impact area, covering 1577 km^2 and accounting for 64.87% of the total study area, as seen in Figure 13d.

Under the action of human activities and natural factors, the landscape structure manifested as three spatial types—perforated, dissected, and fragmented—with landscape patches exhibiting shrinkage or even attrition. Among the matrix types of vegetation cover in the ZJM area, arid grassland is a major species. Calculated as a single ecological type, the FN_1 of the current landscape patch is 0.84, and its fragmentation index is close to 1. Hence, the fragmentation degree of the ZJM landscape is extremely high (You et al., 2006).

5.6 | The socioeconomic value and innovation

The paper mainly made improvements and breakthroughs in the following aspects: The innovation of this paper can be summarized as follow,

- Time resolution of the dataset was improved (the shortest time interval is 3 years) and the time scope of ecological monitoring was increased from 1975 to 2018, up to 44 years. It not only enhance the reliability of the results,

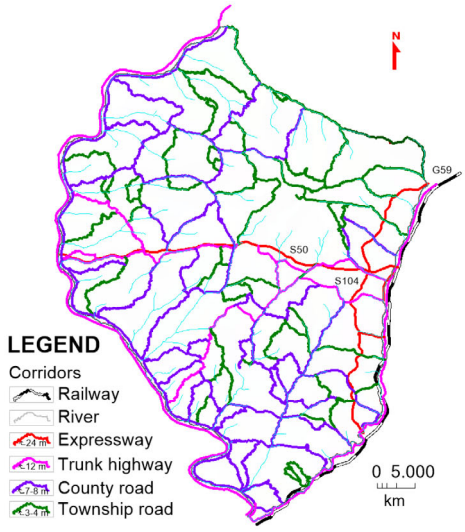

(a) Remote sensing-based road interpretation

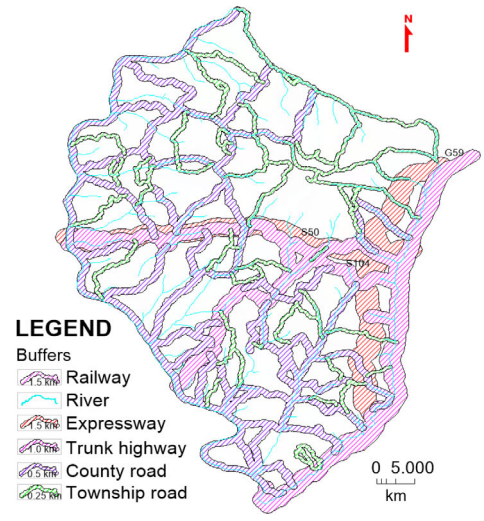

(b) Buffer analysis of various roads

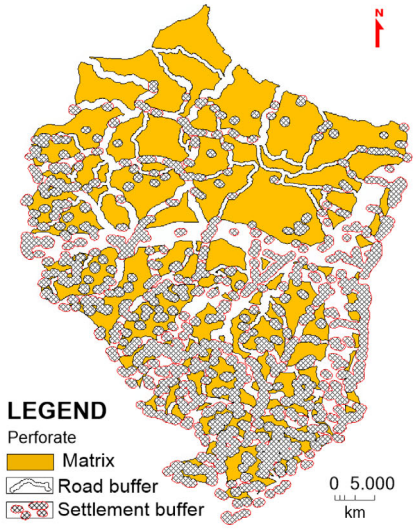

(c) Determination of residential area buffer zone

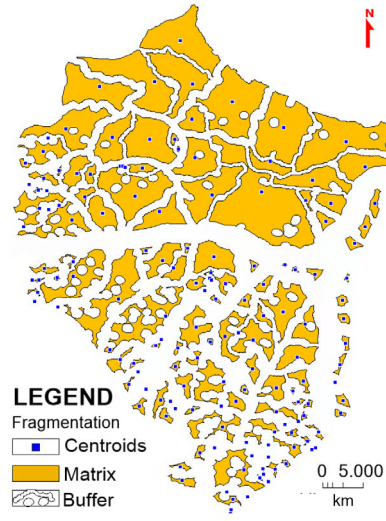

(d) Broken matrix formed by the superimposed influence of valleys, roads, and residential areas

FIGURE 13 Buffer analysis of roads and settlements in the Zijin Mountain area

but also develop the expressiveness of the monitoring results on the long-term evolution feature in the ecological environment.

- Based on landscape cutting caused by soil erosion on the Loess Plateau, the landscape fragmentation caused by natural and human factors in ZJM area was evaluated from the perspectives of road ecology and landscape ecology. And it was found that the superposition of roads aggravated the landscape fragmentation, which in turn lead to the loss of wildlife habitat.
- Combining with the "2030 Sustainable Development Goals, SDGs," the multi-factor comprehensive evaluation index system for poverty-stricken mountain resources and environments has been constructed. It provides

scientific support indicators for China to implement the "2030 Agenda" and to evaluate the effect of targeted poverty alleviation in contiguous destitute areas.

Its socioeconomic values are mainly evident in the following:

- The ZJM area is located in Lvliang a concentrated destitute mountainous area, and this imbalance between economic construction and ecological fragility will lead to a series of problems such as environmental pollution, habitat loss or fragmentation, and productivity decline etc. Considering three objective ecological indicators (NDBI, Night light index, and Landscape Index), we suggest that developing countries should pay attention to ecological and environmental protection while pursuing poverty alleviation and establish a sustainable human settlement environment in rural.
- Eradicating extreme poverty, one of three main aspects such as society, economy, and ecological environment covered by the "2030 Agenda," is the biggest challenge in developing countries and a necessary condition for achieving sustainable development. Over-exploitation of natural resources will destroy the original ecological structure. NDVI and LUCC were used to exhibited human-driven changes in the inland ecological structure and quality and was used to provide scientific references for to realize the SDG-6 (water and sanitation), SDG-11 (cities and human settlements), SDG-13 (climate change), and SDG-15 (protection and restoration of sustainable terrestrial ecosystems).

Research results of this article will be helpful to evaluate the effect of targeted poverty alleviation of concentrated destitute typical area in China, and to understand the problems existing in the sustainable management of regional natural resources.

6 | CONCLUSIONS AND POLICY IMPLICATIONS

Referring to the SDGs (SDG-6, SDG-11, SDG-13, and SDG-15) established by the framework of the 2030 Agenda, this study used multi-temporal remote sensing technology to examine six time series indicators, that is, the NDBI, light brightness index, NDVI, LUCC, climate change, and landscape index, with the belief that these six representative objective indicators could be used to reflect the vulnerability of the ecological environment in the ZJM area (Table 7).

- The NDBI, night light index, and landscape index time series reflected the trend of increasing human activities and urbanization. Over the 44a study period, the area of residential construction land increased at a moderate level, the road density increased by 8.57 times, and the fragmentation of the landscape was extremely high due to human activities. The 22a night light index increased markedly, and the urbanization trend grew. IBM SPSS© correlation analysis revealed that the NDVI was significantly correlated with the night light index of human activity elements (the SPSS© Pearson correlation coefficient was $r = .835$, significance test $p < .02$).
- The climate change time series reflected the fact that the ZJM area has had a warm-humid tendency. In 36 years, the temperature and precipitation increased considerably, and the number of consecutive extreme weather events such as floods and droughts also increased (Rong et al., 2018). The SPSS© correlation analysis indicated that the NDVI was significantly correlated with changes in temperature factors (the SPSS© Pearson correlation coefficient was $r = .721$, significance test $p < .02$).
- The NDVI and LUCC time series reflected regional surface vegetation cover and land use/cover status. Compared with 1987, the average vegetation index in ZJM area increased moderately. The growth of forest land in 2018 was extremely high, and sustainable forest management was better. Dry grassland was progressing well, and the area of bare land is continuing to decrease, and the degree of green exhibited an obvious improvement trend. This

TABLE 7 Evaluation results of resource and environmental dynamic response indicators in the Zijin Mountain area

Goals	Targets (from the 2030 Agenda)	Monitoring results	Indicators and interpretation	Degree
SDG-6 Water and sanitation	6.4 Total length of the water system in the study area (km)	756.2 km	6.4.1 Measures the overall situation of the surface water system in the region.	High
	6.6 Density of the water system per unit area (km/km^2)	0.31 km/km^2	6.6.1 Measures the distribution of surface water systems in the region.	Low
SDG-11 Cities and human settlements	11.3 22a Light index growth multiple	26.9 times	11.3.1 Measures the degree of regional urbanization.	Extremely high
	11.3 44a Residential construction land growth multiple	4.29 times	11.3.2 Measures the characteristics of human activities in the region.	Moderate
SDG-13 Climate change	13.b 36a Temperature growth rate (°C/10a)	0.42°C/10a	13.b.1 Measures the degree of regional temperature changes.	High
	13.b 36a Precipitation growth rate (mm/10a)	18.7 mm/10a	13.b.2 Measures the extent of regional precipitation changes.	High
SDG-15 Terrestrial ecosystems, forests, and desertification	15.1 32a Percentage reduction in area occupied by bare land (%)	32.5%	15.1.1 Measures the greening of bare land in the region.	Moderate
	15.1 32a Percentage increase in the area of arid grassland (%)	40.7%	15.1.2 Measures the progress of regional dry grassland management.	Moderate
	15.2 32a Percentage increase in the area of forest (%)	85.7%	15.2.1 Measures progress in regional sustainable forest management.	Extremely high
SDG-15 Biodiversity	15.4 32a Average vegetation index increase (%)	54.7%	15.4.1 Measures regional biodiversity coverage.	Moderate
	15.5 32a Mountain ecosystem landscape fragmentation growth multiple	6.81 times	15.5.1 Measures the pressure of regional road development on the ecological environment.	Extremely high

Abbreviation: SDG, sustainable development goal.

is in contrast to the "Grain for Green Program", the "Three-North Shelterbelt Program", and other national key ecological protection and restoration projects, which are inseparable (J. J. Li et al., 2017; Q. Wang et al., 2014).

- Studies have shown that the ZJM area has been transformed from an original mountain grassland ecosystem to a mountainous arid agricultural ecosystem. Human activities have modified the original ecological structure and accelerated the fragmentation of habitats. Due to the twin nature of economic poverty and ecological fragility, the decline in many ecological indicators of the ZJM area indirectly reflects the fact that humans still rely heavily on basic natural resources, and their social economy remains a low-level mountain farming economy.

At present, the "ecological environmental protection and high-quality development of the Yellow River Basin" has become a major national strategy (Xi, 2019; F. Wang et al., 2020). Facing the dire combination of serious soil erosion, a fragile ecological environment, ecosystem degradation, and a concentration of multiple poor counties, to ensure the sustainable use of natural resources and the harmony between man and the natural landscape, this study puts forward the following recommendations:

- Lvliang Mountain is located in a poverty-stricken mountainous area far inland on the Loess Plateau in the middle and lower reaches of the Yellow River Basin. This region still needs to cherish natural resources, while striving to continuously improve its urbanization level and greatly improve its accessibility, thereby making full use of tourism resources such as the natural scenery along the Yellow River, the distinctive rural folklore of the Loess Plateau, and its particular type of agriculture to embark down a unique rural revitalization road.
- The connectivity of the information structure between nature, humanities, and the economy in the basin must be established to avoid the trend of "ecological isolation, cultural isolation, and economic isolation."
- Comprehensive multi-perspective and multi-disciplinary integration technology should be developed, natural and human environment evolution should be optimized and innovated, and evaluation and prediction models should be created and utilized, all to achieve harmony between man and the natural landscape, as well as sustainable development.

REFERENCES

Acheampong, M., Yu, Q. Y., Enomah, L. D., Anchang, J., & Eduful, M. (2018). Land use/cover change in Ghana's oil city: Assessing the impact of neoliberal economic policies and implications for sustainable development goal number one-A remote sensing and GIS approach. *Land Use Policy*, *73*(4), 373–384.

Anderson, K., Ryan, B., Sonntag, W., Kavvada, A., & Friedl, L. (2017). Earth observation in service of the 2030 Agenda for Sustainable Development. *Geo-spatial Information Science*, *20*(2), 77–96.

Benítez-López, A., Alkemade, R., & Verweij, P. A. (2010). The impacts of roads and other infrastructure on mammal and bird populations: A meta-analysis. *Biological Conservation*, *143*(6), 1307–1316.

Boarman, W. I., & Sazaki, M. (2006). A highway's road-effect zone for desert tortoises (*Gopherus agasazii*). *Journal of Arid Environments*, *65*(2), 94–101.

Campbell, B. M., Hansen, J., Rioux, J., Stirling, C. M., Twomlow, S., & Wollenberg, E. (2018). Urgent action to combat climate change and its impacts (SDG 13): Transforming agriculture and food systems. *Current Opinion in Environmental Sustainability*, *34*(5), 13–20.

Dong, S. C., Wu, Y. P., & Wang, H. Y. (2003). A study on the eco-economic development model in the eco-environmental vulnerable and needy region on Loess Plateau: The case of Dingxi Prefecture in Gansu Province. *Geographical Research*, *22*(5), 590–600 (in Chinese).

Du, Q. Q., Zhang, M. J., Wang, S. J., Che, C. W., Qiu, X., & Ma, Z. Z. (2018). Changes in air temperature of China in response to global warming hiatus. *Acta Geographica Sinica*, *73*(9), 1748–1764 (in Chinese).

Du, Z. G. (2018). Evaluation and countermeasures of the development level of new urbanization in Shanxi province. *Chinese Journal of Agricultural Resources and Regional Planning*, *39*(6), 122–127 (in Chinese).

Ehrensperger, A., Bremond, A. D., Providoli, I., & Messerli, P. (2019). Land system science and the 2030 agenda: Exploring knowledge that supports sustainability transformation. *Current Opinion in Environmental Sustainability*, *38*(3), 68–76.

Fang, C. L., & Wang, Y. (2015). A comprehensive assessment of urban vulnerability and its spatial differentiation in China. *Acta Geographica Sinica*, *70*(2), 234–247 (in Chinese).

Feng, T., Wu, X. M., & Zhang, H. F. (2019). Distribution of ungulate in different grades of highway and influential factors concerned in Qinling Mountains. *Shaanxi Forest Science and Technology*, *47*(5), 1–6 (in Chinese).

Fernandes, P., Vilaça, M., Macedo, E., Sampaio, C., Bahmankhah, B., Bandeira, J. M., Guarnaccia, C., Rafael, S., Fernandes, A. P., Relvas, H., Borrego, C., & Coelho, M. C. (2019). Integrating road traffic externalities through a sustainability indicator. *Science of the Total Environment*, *691*(48), 483–498.

Hao, X. P. (2011). *Biodiversity of plant communities under different habitats in Heichashan mountain natural reserve, Shanxi province* (Chinese Master's Theses) Full-text Database, No.S1, Basic Sciences, A006-327-13-14 (in Chinese).

Holloway, J., & Mengersen, K. (2018). Statistical machine learning methods and remote sensing for sustainable development goals: A review. *Remote Sensing*, *10*(9), 1365.

Hu, Z. J., Yu, C. Q., Xu, H. F., & Wang, Y. (2005). Ecological effects of roads on terrestrial animals. *Chinese Journal of Ecology*, *24*(4), 433–437 (in Chinese).

IPCC. (2013). *Climate change 2013: The physical science basis. Contribution to Working Group I to the Fifth Assessment Report of the Intergovernmental Panel on Climate Change*. Cambridge University Press.

Juwana, I., Muttil, N., & Perera, B. J. C. (2016). Uncertainty and sensitivity analysis of West Java Water Sustainability Index-A case study on Citarum catchment in Indonesia. *Ecological Indicators*, *61*(3), 170–178.

Kussul, N., Lavreniuk, M., Kolotii, A., Skakun, S., Rakoid, O., & Shumilo, L. (2020). A workflow for Sustainable Development Goals indicators assessment based on high-resolution satellite data. *International Journal of Digital Earth*, *13*(2), 309–321.

Lambin, E. F., Baulies, X., Bockstael, N., Fischer, G., Krug, T., Leemans, R., Moran, E. F., Rindfuss, R. R., Sato, Y., Skole, D., Turner II, B. L., & Vogel, C. (1999). *Land-use and land-cover change (LUCC): Implementation strategy* (IGBP Report 48/IHDP Report 10).

Li, D. R., & Li, X. (2015). An overview on data mining of nighttime light remote sensing. *Acta Geodaetica et Cartographica Sinica*, *44*(6), 591–601 (in Chinese).

Li, F., Zhang, J. X., & Zhang, R. (2015). Spatial-temporal characteristics of precipitation in Shanxi during 1958–2013. *Journal of Desert Research*, *35*(5), 1301–1311 (in Chinese).

Li, J. J., Peng, S. Z., & Li, Z. (2017). Detecting and attributing vegetation changes on China's Loess Plateau. *Agricultural and Forest Meteorology*, *247*(13), 260–270.

Li, M. Y., Zhou, Q., Huang, W. Q., & Liu, F. (2012). Geomatics—Based analysis of landscape security pattern for wild animals in eastern suburb of Nanjing city – A case study of *Hydropotes inermis*. *Journal of Southwest Forestry University (Natural Science)*, *32*(4), 70–75 (in Chinese).

Li, S., Zhang, X. F., Shi, J. B., Dong, S. K., & Gao, X. X. (2018). Effects of highway from Inner Mongolia to Xinjiang on habitat suitability of ungulates in Alashan desert. *Chinese Journal of Ecology*, *37*(1), 103–110 (in Chinese).

Li, X. M., & Zhou, W. Q. (2018). Dasymetric mapping of urban population in China based on radiance corrected DMSP-OLS nighttime light and land cover data. *Science of the Total Environment*, *643*(25), 1248–1256.

Li, Z. G., Wang, Y. L., Zhang, X. F., & Wu, J. S. (2005). Spatial-temporal dynamics of landscape fragmentation in North Shannxi Loess Plateau. *Chinese Journal of Applied Ecology*, *16*(11), 2066–2070 (in Chinese).

Liu, J. Y., Ning, J., Kuang, W. H., Xu, X. L., Zhang, S. W., Yan, C. Z., Li, R. D., Wu, S. X., Hu, Y. F., Du, G. M., Chi, W. F., Pan, T., & Ning, J. (2018). Spatio-temporal patterns and characteristics of land-use change in China during 2010–2015. *Acta Geographica Sinica*, *73*(5), 789–802 (in Chinese).

Liu, L. B., Wang, Z., Wang, Y., Zhang, Y. T., Shen, J. S., Qin, D. H., & Li, S. C. (2019). Trade-off analyses of multiple mountain ecosystem services along elevation, vegetation cover and precipitation gradients: A case study in the Taihang Mountains. *Ecological Indicators*, *103*(9), 94–104.

Lu, Y. L., Yuan, J. J., Lu, X. T., Su, C., Zhang, Y. Q., Wang, C. C., Cao, X. H., Li, Q. F., Su, J. L., Ittekkot, V., Garbutt, R. A., Bush, S., Fletcher, S., Wagey, T., Kachur, A., & Sweijd, N. (2018). Major threats of pollution and climate change to global coastal ecosystems and enhanced management for sustainability. *Environmental Pollution*, *239*(8), 670–680.

Madadi, H., Moradi, H., Soffianian, A., Salmanmahiny, A., Senn, J., & Geneletti, D. (2017). Degradation of natural habitats by roads: Comparing land-take and noise effect zone. *Environmental Impact Assessment Review*, *65*(4), 147–155.

Mallick, P. H., & Chakraborty, S. K. (2018). Forest, wetland and biodiversity: Revealing multi-faceted ecological services from ecorestoration of a degraded tropical landscape. *Ecohydrology & Hydrobiology*, *18*(3), 278–296.

Muradyan, V., Tepanosyan, G., Asmaryan, S., Saghatelyan, A., & Dell'Acqua, F. (2019). Relationships between NDVI and climatic factors in mountain ecosystems: A case study of Armenia. *Remote Sensing Applications: Society and Environment*, *14*(2), 158–169.

Myneni, R. B., Dong, J., Tucker, C. J., Kaufmann, R. K., Kauppi, P. E., Liski, J., Zhou, L., Alexeyev, V., & Hughes, M. K. (2001). A large carbon sink in the woody biomass of northern forests. *Proceedings of the National Academy of Sciences*, *98*(26), 14784–14789.

Parsa, V. A., Salehi, E., Yavari, A. R., & Bodegom, P. M. V. (2019). Analyzing temporal changes in urban forest structure and the effect on air quality improvement. *Sustainable Cities and Society*, *48*(5), 101548.

Qi, X. X., & Dang, H. P. (2018). Addressing the dual challenges of food security and environmental sustainability during rural livelihood transitions in China. *Land Use Policy*, *77*(8), 199–208.

Qi, X. X., Wang, R. Y., Li, J. C., Zhang, T., Liu, L. M., & He, Y. L. (2018). Ensuring food security with lower environmental costs under intensive agricultural land use patterns: A case study from China. *Journal of Environmental Management*, *213*(9), 329–340.

Qin, D. H., Stocker, T., & 259 Authors and TSU (Bern and Beijing). (2014). Highlights of the IPCC Working Group I fifth assessment report. *Progressus Inquisitiones De Mutatione Climatis*, *10*(1), 1–6 (in Chinese).

Rong, X. Q., Pang, J. L., & Han, J. Q. (2018). Distribution trends of drought and flood disasters and climate background from 1958 to 2012 in Shanxi province. *Journal of Arid Land Resources and Environment*, *32*(9), 97–102 (in Chinese).

Schirpke, U., Kohler, M., Leitinger, G., Fontana, V., Tasser, E., & Tappeiner, U. (2017). Future impacts of changing land-use and climate on ecosystem services of mountain grassland and their resilience. *Ecosystem Services*, *26*(4), 79–94.

Schmeller, D. S., Loyau, A., Bao, K., Bracke, W., Chatzinotas, A., Vleeschouwer, F. D., Friesen, J., Gandois, L., Hansson, S. V., Haver, M., Le Roux, G., Shen, J., Teisserenc, R., & Vredenburg, V. T. (2018). People, pollution and pathogens–Global change impacts in mountain freshwater ecosystems. *Science of the Total Environment*, *622–623*(9), 756–763.

Sun, R., Chen, S. H., & Su, H. B. (2019). Spatio-temporal variations of NDVI of different land cover types on the Loess Plateau from 2000 to 2016. *Progress in Geography*, *38*(8), 1248–1258 (in Chinese).

Turner, B. L., Moss, R. H., & Skole, D. L. (1993). Relating land use and global land-cover change: A proposal for an IGBP-IHDP core project. In *Report from the IGBP-IHDP Working Group on Land-Use/Land-Cover Change* (IGBP Report 24/IHDP Report 5). Royal Swedish Academy of Sciences.

United Nations. (2015). *Transforming our world: The 2030 agenda for sustainable development*, *A/RES/70/1*. https://sustainabledevelopment.un.org/post2015/transformingourworld

Van der Ree, R., Jaeger, J. A. G., van der Grift, E. A., & Clevenger, A. P. (2011). Effects of roads and traffic on wildlife populations and landscape function: Road ecology is moving toward larger scales. *Ecology and Society*, *16*(1), 48.

Virto, L. R. (2018). A preliminary assessment of the indicators for Sustainable Development Goal (SDG) 14 Conserve and sustainably use the oceans, seas and marine resources for sustainable development. *Marine Policy*, *98*(12), 47–57.

Visbeck, M., Kronfeld-Goharani, U., Neumann, B., Rickels, W., Schmidt, J., Doorn, E., Matz-Lück, N., & Proelss, A. (2014). A sustainable development goal for the ocean and coasts: Global ocean challenges benefit from regional initiatives supporting globally coordinated solutions. *Marine Policy*, *49*(7), 87–89.

Vörösmarty, C. J., Osuna, V. R., Cak, A. D., Bhaduri, A., Bunn, S. E., Corsi, F., Gastelumendi, J., Green, P., Harrison, I., Lawford, R., Marcotullio, P. J., McClain, M., McDonald, R., McIntyre, P., Palmer, M., Robarts, R. D., Szöllösi-Nagy, A., Tessler, Z., & Uhlenbrook, S. (2018). Ecosystem-based water security and the Sustainable Development Goals (SDGs). *Ecohydrology & Hydrobiology*, *18*(4), 317–333.

Wang, F., An, L. Z., Dang, A. R., Han, J. Y., Miao, C. H., Wang, J., Zhang, G. H., & Zhao, Y. (2020). Human-land coupling and sustainable human settlements in the Yellow River Basin. *Geographical Research*, *39*(8), 1707–1724 (in Chinese).

Wang, H., Yan, J. Z., & Li, H. L. (2018). Forest transition and its explanation in contiguous destitute areas of China. *Acta Geographica Sinica*, *73*(7), 1253–1267.

Wang, M. B., & Fan, X. H. (2009). Characterization of general change patterns of air temperature and precipitation over the 50 years from 1959 to 2008 in Shanxi Province, China. *Journal of Shanxi University (Natural Science Edition)*, *32*(4), 640–648 (in Chinese).

Wang, Q., Zhang, B., Zhang, Z. Q., Zhang, X. F., & Dai, S. P. (2014). The three-north shelterbelt program and dynamic changes in vegetation cover. *Journal of Resources and Ecology*, *5*(1), 53–59.

Xi, J. P. (2019). Speech at the symposium on ecological protection and high—Quality development of the Yellow River Basin. *China Water*, *20*, 1–3.

Xu, X., Xie, Y. J., Qi, K., Luo, Z. K., & Wang, X. R. (2018). Detecting the response of bird communities and biodiversity to habitat loss and fragmentation due to urbanization. *Science of the Total Environment*, *624*(10), 1561–1576.

Xu, X. B., Hu, H. Z., Tan, Y., Yang, G. S., Zhu, P., & Jiang, B. (2019). Quantifying the impacts of climate variability and human interventions on crop production and food security in the Yangtze River Basin, China, 1990–2015. *Science of the Total Environment*, *665*(22), 379–389.

Yang, J., & Zhao, Y. X. (2015). Comprehensive evaluation of urbanization level of countits in Shanxi Province and its developmental countermeasures. *Acta Agriculturae Jiangxi*, *27*(3), 117–122 (in Chinese).

Yin, H., & Sun, Y. (2018). Characteristics of extreme temperature and precipitation in China in 2017 based on ETCCDI indices. *Advances in Climate Change Research*, *9*(4), 218–226.

You, C., Zhou, Y. B., & Yu, L. F. (2006). An introduction of quantitative methods in landscape pattern fragmentation. *Chinese Agricultural Science Bulletin*, *22*(5), 146–151 (in Chinese).

Zhang, Q. L., Pandey, B., & Seto, K. C. (2016). A robust method to generate a consistent time series from DMSP/OLS nighttime light data. *IEEE Transactions on Geoscience and Remote Sensing*, *54*(10), 5821–5831.

Zhang, W. Q., Sun, C. J., & Li, X. G. (2019). Vegetation cover change and ecological effect assessment in the Loess Plateau of Southwest Shanxi province based on remote sensing image. *Journal of Natural Resources*, *34*(8), 1748–1758 (in Chinese).

Zhao, X., Sun, H. B., Chen, B., Xia, X. H., & Li, P. F. (2019). China's rural human settlements: Qualitative evaluation, quantitative analysis and policy implications. *Ecological Indicators*, *105*(11), 398–405.

Zhou, Q., Wu, Y. H., Dong, Z. F., Li, H. X., & Ge, C. Z. (2018). Analysis and revelation of sustainable development goals index and dashboards report 2017. *Environmental Protection*, *46*(20), 63–69 (in Chinese).

Zhou, X. Y., Lei, K., & Meng, W. (2017). An approach of habitat degradation assessment for characterization on coastal habitat conservation tendency. *Science of the Total Environment*, *593–594*(16), 618–623.

Zhou, Y., Huang, X. J., Chen, Y., Zhong, T. Y., Xu, G. L., He, J. L., Xu, Y. T., & Meng, H. (2017). The effect of land use planning (2006–2020) on construction land growth in China. *Cities*, *68*(10), 37–47.

How to cite this article: Huang, S., Ma, C., & Liu, P. (2022). Responses of sustainable development indicators to human activities and climate change in ecologically fragile areas of impoverished counties in China. *Natural Resources Forum*, 1–31. https://doi.org/10.1111/1477-8947.12263